Progress In Electromagnetics Research, PIER 92, 281–298, 2009

TRANSIENT ANALYSIS OF WIRE STRUCTURES USING TIME DOMAIN INTEGRAL EQUATION METHOD WITH EXACT MATRIX ELEMENTS

G. H. Zhang, M. Y. Xia, and X. M. Jiang

School of Electronics Engineering and Computer Science
Peking University
Beijing 100871, China

Abstract—A novel time-domain integral equation (TDIE) solver for transient analysis of conducting wires is proposed. It is formulated using the distribution of induced electric dipoles as unknown function. The triangular and B-spline functions are employed as the spatial and temporal basis functions, respectively. By using these basis functions, the matrix elements are found obtainable via exact closed-form formulae, which furnish a robust scheme in terms of stability and accuracy. In addition, to accelerate the matrix filling, a recursive algorithm is introduced. Numerical validations are provided by a dipole antenna, a V-shape antenna and a helical antenna.

1. INTRODUCTION

Time domain integral equation (TDIE) method has proven an appealing alternative to the popular finite-difference time-domain (FDTD) method for transient analyses [1–4]. The advantages of TDIE method include solution of fewer unknowns using surface discretization and elimination of artificial absorbing boundary conditions (ABC) for open-region problems. The efficiency of TDIE method is also well recognized due to the marching-on-in-time (MOT) scheme, which may be further accelerated by fast techniques such as the plane-wave time-domain (PWTD) algorithm [5] and the adaptive integral method (AIM) [6]. The underlying drawback that impedes the prevalence of the TDIE method is the lack of an explicit stability condition like the Courant condition in FDTD method [7].

Corresponding author: M. Y. Xia (myxia@pku.edu.cn).

To suppress the late-time instability, many measures have been attempted, including the filtering or averaging techniques [8, 9], the implicit schemes [10, 11], the use of Galerkin matching in temporal domain [12] or marching-on-in-degree (MOD) approach [13], the varying combination of governing equations [14, 15], the proper choice of temporal basis functions [16–19], and the accurate evaluation of matrix elements by analytical integration in part [20–23], etc. Among these procedures, by our experience, the accurate evaluation of matrix elements seems to be most dependable in both stability and accuracy. This urges us to develop exact techniques for calculations of full matrix elements to promote the TDIE methods.

Conventionally, Galerkin matching is adopted in spatial domain, while point matching is adopted in temporal domain. Under these matching ways, the calculations of matrix elements are double integrals over the source and observation regions, where the double integrals are actually quadruple integrals for surface-modeling 3D bodies. The complexity of the double integrals involves the choices of both spatial and temporal basis functions. The triangular basis functions for wire structures or RWG basis functions [24] for arbitrarily-shaped 3D bodies are widely employed as the spatial basis functions, while piecewise-defined polynomials are largely chosen as temporal basis functions [18, 19]. Exact closed-form formulae for calculations of full matrix elements that involve RWG bases (suiting surface-modeling 3D bodies) seem to be impossible. However, analytical calculations of full matrix elements that involve triangular bases (suiting segment-modeling wire structures) are very likely and deserve to be explored. This is the purpose of the present work. It is expected that the proposed approach based on exact matrix elements would be immune to instability without sacrifice of accuracy or efficiency, unlike using the implicit formulation that loses accuracy or using Galerkin matching in temporal domain that pushes aside the efficient MOT scheme.

The paper is organized as follows. Theory framework is outlined in Section 2. Section 3 is dedicated to derivation of closed-form formulae for calculations of matrix elements. Numerical demonstrations are provided in Section 4. Section 5 contains a few concluding remarks.

2. FORMULATION

Refer to Figure 1 and consider a transient wave incident upon an arbitrarily-curved conducting wire Γ, which induces a distribution of electric dipoles $\mathbf{P}$ along the wire. The induced currents and charges on the wire are related to $\mathbf{P}$ through $\mathbf{I}(\mathbf{r}', t') = \partial \mathbf{P}(\mathbf{r}', t')/\partial t'$ and $\sigma(\mathbf{r}', t') = -\nabla' \cdot \mathbf{P}(\mathbf{r}', t')$, where ∇' is to differentiate with respect to the

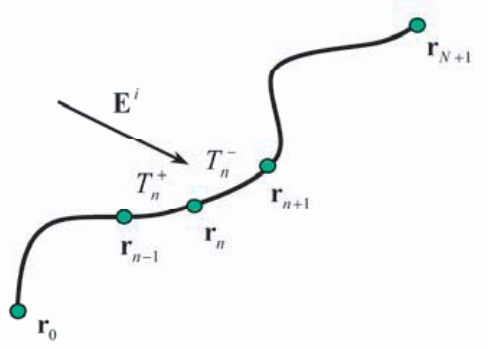

Figure 1. Geometry of transient scattering by a thin wire.

length along the wire. The Hertz vector potential and electric scalar potential generated by the induced sources $\mathbf{P}$ are

$$\mathbf{\Pi}(\mathbf{r},t) = \frac{1}{4\pi\varepsilon_0}\int_\Gamma \frac{dl'}{R}\left[\mathbf{P}\left(\mathbf{r}',t'\right)\right]_{t'=t-R/c} \tag{1}$$

$$\phi(\mathbf{r},t) = \frac{1}{4\pi\varepsilon_0}\int_\Gamma \frac{dl'}{R}\left[-\nabla'\cdot\mathbf{P}\left(\mathbf{r}',t'\right)\right]_{t'=t-R/c} \tag{2}$$

where $R = |\mathbf{r}-\mathbf{r}'|$ is the distance from the source point $\mathbf{r}'$ to the observation point $\mathbf{r}$. The scattered electric fields can be expressed by the potentials as:

$$\mathbf{E}^s = -\frac{\partial^2\mathbf{\Pi}}{\partial(ct)^2} - \nabla\phi \tag{3}$$

The boundary conditions on the conducting wire demands:

$$\left[\mathbf{E}^i + \mathbf{E}^s\right]_{\tan} = \mathbf{0} \tag{4}$$

where $[*]_{\tan}$ means taking the tangential component along the wire.

Suppose that there is neither charge nor current on the wire before the instant $t' = 0$, that is, $\mathbf{P}(\mathbf{r}',t') = \partial\mathbf{P}(\mathbf{r}',t')/\partial t' = 0$ for $t' \le 0$. Expand $\mathbf{P}(\mathbf{r}',t')$ using the triangular functions in spatial domain and the quadratic B-pline functions in temporal domain:

$$\mathbf{P}(\mathbf{r}',t') = (4\pi\varepsilon_0)\sum_{j=1}^{\infty}\sum_{n=1}^{N} c_n(j)\mathbf{f}_n\left(\mathbf{r}'\right)T\left(\bar{t}'-j\right) \tag{5}$$

where $\bar{t}' = t'/\Delta t$ with Δt being the time-step size, N is the number of interior nodes of the segmented wire. The triangular basis functions

defined on the wire are

$$\mathbf{f}_n(\mathbf{r}') = \begin{cases} \mathbf{f}_n^+(\mathbf{r}') = \dfrac{\mathbf{r}' - \mathbf{r}_{n-1}}{l_n^+}, \ \mathbf{r}' \in T_n^+ \\ \mathbf{f}_n^-(\mathbf{r}') = \dfrac{\mathbf{r}_{n+1} - \mathbf{r}'}{l_n^-}, \ \mathbf{r}' \in T_n^- \end{cases} \tag{6}$$

where $l_n^+ = |\mathbf{r}_n - \mathbf{r}_{n-1}|$ and $l_n^- = |\mathbf{r}_{n+1} - \mathbf{r}_n|$ are the lengths of the segments T_n^+ and T_n^-, respectively. The quadratic B-spline function is [18]:

$$T\left(\bar{t}'\right) = \begin{cases} \dfrac{1}{2}\left(\bar{t}' + 1\right)^2, & 0 \le \bar{t}' + 1 < 1 \\ \dfrac{1}{2} + \bar{t}' - \bar{t}'^2, & 0 \le \bar{t}' < 1 \\ \dfrac{1}{2} - \left(\bar{t}' - 1\right) + \dfrac{1}{2}\left(\bar{t}' - 1\right)^2, & 0 \le \bar{t}' - 1 < 1 \end{cases} \tag{7}$$

Substituting (5) into (4) with (1)–(3) in places, and then testing (4) by $\mathbf{f}_m(\mathbf{r})\delta(\bar{t} - i)$ $(m = 1, 2, \ldots, N;\ i = 1, 2, 3, \ldots)$, where $\bar{t} = t/\Delta t$, we obtain

$$\sum_{j=1}^{\infty} \sum_{n=1}^{N} Z_{mn}(i-j) c_n(j) = b_m(i) \tag{8}$$

with

$$\begin{aligned} Z_{mn}(j) \ = \ & \int_{T_m} \int_{T_n} \frac{1}{R} \left[\frac{T''\left(j - \bar{R}\right)}{(c\Delta t)^2} \mathbf{f}_m(\mathbf{r}) \cdot \mathbf{f}_n(\mathbf{r}') \right. \\ & \left. + T\left(j - \bar{R}\right) g_m(\mathbf{r}) g_n(\mathbf{r}') \right] dl' dl \end{aligned} \tag{9}$$

$$b_m(i) \ = \ \int_{T_m} \mathbf{f}_m(\mathbf{r}) \cdot \mathbf{E}^i(\mathbf{r}, i\Delta t) dl \tag{10}$$

In (9), $\bar{R} = R/c\Delta t$, $g_m(\mathbf{r}) = -\nabla \cdot \mathbf{f}_m(\mathbf{r})$ and $g_n(\mathbf{r}') = -\nabla' \cdot \mathbf{f}_n(\mathbf{r}')$. Due to the compactness of the temporal basis function, i.e., $-1 \le j - \bar{R} < 2$, $Z_{mn}(j)$ would be nonzero only for $0 \le j \le L$, where $L = \mathrm{int}(\bar{R}_{\max} + 2)$ and $\bar{R}_{\max} = R_{\max}/(c\Delta t)$ with $R_{\max}$ being the maximum linear dimension of the curved wire. By changing the index $i - j \to j$, we can rewrite (8) in the form of the conventional marching-on-in-time (MOT) scheme:

$$[Z(0)]\{c(i)\} = \{b(i)\} - \sum_{j=1}^{\min(i-1, L)} [Z(j)]\{c(i-j)\}, \quad i = 1, 2, 3, \ldots \tag{11}$$

where $[Z(j)]$ $(j = 0, 1, 2, \ldots, L)$ are $N \times N$ interacting matrices, which are very sparse, while $\{b(i)\}$ and $\{c(j)\}$ are $N \times 1$ column vectors.

To fill the system matrices $[Z(j)]$ for $0 \leq j \leq L$ more wisely, we define four integrals:

$$X_{mn}(j) = \frac{1}{(c\Delta t)^2} \int_{T_m} \int_{T_n} \mathbf{f}_m(\mathbf{r}) \cdot \mathbf{f}_n(\mathbf{r}') \frac{\chi\left(j - \bar{R}\right)}{R} dl' dl \tag{12}$$

$$\left\{ \begin{array}{c} Y_{mn}^{(0)}(j) \\ Y_{mn}^{(1)}(j) \\ Y_{mn}^{(2)}(j) \end{array} \right\} = \int_{T_m} \int_{T_n} \left\{ \begin{array}{c} 1 \\ \left(j - \bar{R}\right) \\ \left(j - \bar{R}\right)^2 \end{array} \right\} g_m(\mathbf{r}) g_n(\mathbf{r}') \frac{\chi\left(j - \bar{R}\right)}{R} dl' dl \tag{13}$$

where $\chi\left(j - \bar{R}\right)$ is the characteristic function that reads

$$\chi\left(j - \bar{R}\right) = \left\{ \begin{array}{l} 1, \ 0 \leq j - \bar{R} < 1 \\ 0, \ \text{otherwise} \end{array} \right. \tag{14}$$

Using the definitions of (12)–(13), we find that (9), with (7) in place, can be calculated in a recursive way:

$$\begin{aligned} Z_{mn}(j) \ = \ & \tfrac{1}{2}\tilde{Y}_{mn}^{(2)}(j) + \left[\tfrac{1}{2}Y_{mn}^{(0)}(j-1) + Y_{mn}^{(1)}(j-1) - \tilde{Y}_{mn}^{(2)}(j-1)\right] \\ & + \left[\tfrac{1}{2}Y_{mn}^{(0)}(j-2) - Y_{mn}^{(1)}(j-2) + \tfrac{1}{2}\tilde{Y}_{mn}^{(2)}(j-2)\right] \end{aligned} \tag{15}$$

where $\tilde{Y}_{mn}^{(2)}(j) = Y_{mn}^{(2)}(j) + 2X_{mn}(j)$, and so forth. Evaluating (12)–(13) is more efficient than performing (9), because the supported interval is only one in (12)–(13), while it is three in (9), which means that the number of nonzero elements of $[Y(j)]$ is about one third of that of $[Z(j)]$. Numerical experiments show that filling the matrix entries by using (15) via (12)–(13) saves at least half CPU time than by carrying out (9) directly.

Once the coefficients $\{c(j)\}_{j=0}^{N_t}$ are found recursively by (11), where N_t is the length of the time sequence that has been resolved, the distributions of currents and charges along the wire can be retrieved. The scattered far-field is calculated by the first term of (3) and then just taking the transverse components.

3. DERIVATION OF MATRIX ELEMENTS

Let the unit directional vector of the segment T_m^p and T_n^q be indicated by $\hat{s}_m^p$ and $\hat{s}_n^q$, respectively, where $\hat{s}_m^p$ is defined by $\hat{s}_m^p = (\mathbf{r}_{m+p-1} - \mathbf{r}_{m+p-2})/l_m^p$ (hereafter we let $p = 1$ stands for " $+$ " and $p = 2$ stands

for "$-$"), and so is $\hat{s}_n^q$. Then the spatial basis functions in (6) become $\mathbf{f}_n^q(\mathbf{r}') = l'\hat{s}_n^q$ if $q = 1$ and $\mathbf{f}_n^q(\mathbf{r}') = (l_n^q - l')\ \hat{s}_n^q$ if $q = 2$, for $0 < l' < l_n^q$. We also have $g_n^q(\mathbf{r}') = -\nabla' \cdot \mathbf{f}_n^q(\mathbf{r}') = -(-1)^q/l_n^q$. Substituting these expressions into (12)–(13), we obtain

$$X_{mn}(j) = \frac{1}{(c\Delta t)^2} \sum_{p,q=1}^{2,2} \frac{\hat{s}_m^p \cdot \hat{s}_n^q}{l_m^p l_n^q} F_{m,n}^{p,q}(j) \tag{16}$$

$$\begin{Bmatrix} Y_{mn}^{(0)}(j) \\ Y_{mn}^{(1)}(j) \\ Y_{mn}^{(2)}(j) \end{Bmatrix} = \sum_{p,q=1}^{2,2} \frac{(-1)^{p+q}}{l_m^p l_n^q} \begin{Bmatrix} I_3(l_m^p, l_n^q) \\ jI_3(l_m^p, l_n^q) - \frac{1}{c\Delta t} I_4(l_m^p, l_n^q) \\ j^2 I_3(l_m^p, l_n^q) - \frac{2j}{c\Delta t} I_4(l_m^p, l_n^q) + \frac{1}{(c\Delta t)^2} I_5(l_m^p, l_n^q) \end{Bmatrix} \tag{17}$$

In (16)–(17),

$$F_{m,n}^{p,q}(j) = \begin{cases} I_1(l_m^p, l_n^q),\ p = 1;\ q = 1 \\ l_n^q I_2(l_m^p, l_n^q) - I_1(l_m^p, l_n^q),\ p = 1;\ q = 2 \\ l_m^p I_2'(l_m^p, l_n^q) - I_1(l_m^p, l_n^q),\ p = 2;\ q = 1 \\ l_m^p l_n^q I_3(l_m^p, l_n^q) - l_m^p I_2'(l_m^p, l_n^q) - l_n^q I_2(l_m^p, l_n^q) + I_1(l_m^p, l_n^q),\ p = 2;\ q = 2 \end{cases} \tag{18}$$

with

$$\begin{cases} I_1(l_m^p, l_n^q) = \int_0^{l_m^p} \int_0^{l_n^q} ll' \frac{\chi\left(j - \bar{R}\right)}{R} dl'dl \\ I_2(l_m^p, l_n^q) = \int_0^{l_m^p} \int_0^{l_n^q} l \frac{\chi\left(j - \bar{R}\right)}{R} dl'dl \\ I_2'(l_m^p, l_n^q) = \int_0^{l_m^p} \int_0^{l_n^q} l' \frac{\chi\left(j - \bar{R}\right)}{R} dl'dl \\ I_3(l_m^p, l_n^q) = \int_0^{l_m^p} \int_0^{l_n^q} \frac{\chi\left(j - \bar{R}\right)}{R} dl'dl \\ I_4(l_m^p, l_n^q) = \int_0^{l_m^p} \int_0^{l_n^q} \chi\left(j - \bar{R}\right) dl'dl \\ I_5(l_m^p, l_n^q) = \int_0^{l_m^p} \int_0^{l_n^q} R\chi\left(j - \bar{R}\right) dl'dl \end{cases} \tag{19}$$

These integrals can be cast into the general form

$$I(l_m^p, l_n^q) = \int_0^{l_m^p} \int_0^{l_n^q} h(l, l')\chi\left(j - \bar{R}\right) dl' dl \tag{20}$$

where $h(l, l')$ takes one of the five cases: $h(l, l') = \frac{l'l}{R}$, $\frac{l'}{R}$ or $\frac{l}{R}$, $\frac{1}{R}$, 1, R. One may show that, if it were not for $\chi\left(j - \bar{R}\right)$ that imposes the causality constraint, the integrals in (19) could be carried out analytically, so that we would obtain closed-form expressions for full of the matrix elements. Therefore, we will focus on resolving the causality by transferring the constraint to the limits of integration.

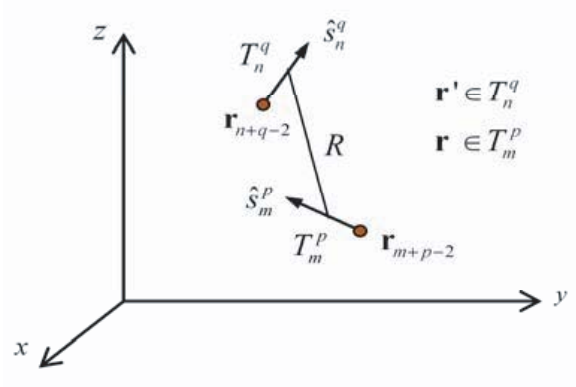

Figure 2. The distance between the observation and source points.

As shown in Figure 2, let R denote the distance between the observation point $\mathbf{r}$ and the source point $\mathbf{r}'$, where $\mathbf{r}$ is on the segment T_m^p while $\mathbf{r}'$ is on the segment T_n^q. We can write out $\mathbf{r} = \mathbf{r}_{m+p-2} + l\hat{s}_m^p$ $(p = 1, 2)$ for $0 \le l \le l_m^p$ and $\mathbf{r}' = \mathbf{r}_{n+q-2} + l'\hat{s}_n^q$ $(q = 1, 2)$ for $0 \le l' \le l_n^q$. Using the thin-wire approximation, i.e., the observer is considered on the surface of the wire while the source is taken to be concentrated on and flowing along the central axis of the wire, we have

$$\begin{aligned} R &= \left|\tilde{\mathbf{r}} - \mathbf{r}'\right|, \ \tilde{\mathbf{r}} = \mathbf{r} + a\hat{\tau} \\ &= \left|(\tilde{\mathbf{r}}_{m+p-2} + l\hat{s}_m^p) - (\mathbf{r}_{n+q-2} + l'\hat{s}_n^q)\right|, \ \tilde{\mathbf{r}}_{m+p-2} = \mathbf{r}_{m+p-2} + a\hat{\tau} \\ &= \sqrt{[l' - P(l)]^2 + A(l)} = \sqrt{[l - Q(l')]^2 + B(l')} \end{aligned} \tag{21}$$

where a is the radius while $\hat{\tau}$ is a unit directional vector that is perpendicular to the axis, and

$$\begin{cases} P(l) = \alpha l - \xi, \ A(l) = \left(1 - \alpha^2\right) l^2 + 2\left(\alpha\xi + \eta\right) l + \left(d^2 - \xi^2\right) \\ Q\left(l'\right) = \alpha l' - \eta, \ B\left(l'\right) = \left(1 - \alpha^2\right) l'^2 + 2\left(\alpha\eta + \xi\right) l' + \left(d^2 - \eta^2\right) \end{cases} \tag{22}$$

with $\alpha = \hat{s}_m^p \cdot \hat{s}_n^q$, $\xi = \hat{s}_m^p \cdot (\tilde{\mathbf{r}}_{m+p-2} - \mathbf{r}_{n+q-2})$, $\eta = \hat{s}_n^q \cdot (\mathbf{r}_{n+q-2} - \tilde{\mathbf{r}}_{m+p-2})$, and $d = |\tilde{\mathbf{r}}_{m+p-2} - \mathbf{r}_{n+q-2}|$.

Substituting (21) into the function $\chi\left(j - \bar{R}\right)$ defined in (14), we have

$$0 \le j - \bar{R} < 1 \Leftrightarrow \ (j-1)c\Delta t < \sqrt{[l' - P(l)]^2 + A(l)} \le jc\Delta t \tag{23}$$

from which we can solve for l' to get

$$\begin{cases} P(l) - U_j(l) \le l' < P(l) - \tilde{U}_{j-1}(l), \text{ or} \\ P(l) + \tilde{U}_{j-1}(l) < l' \le P(l) + U_j(l) \end{cases} \tag{24}$$

where

$$\tilde{U}_{j-1}(l) = \begin{cases} \sqrt{u_{j-1}^2 - A(l)}, & \text{if } A(l) \le u_{j-1}^2 \\ 0, & \text{if } A(l) > u_{j-1}^2 \end{cases} \tag{25}$$

$$U_j(l) = \begin{cases} \sqrt{u_j^2 - A(l)}, & \text{if } A(l) \le u_j^2 \\ \text{non-causal}, & \text{if } A(l) > u_j^2 \end{cases} \tag{26}$$

with $u_j = j(c\Delta t)$ $(j \ge 0)$. Similarly, the solution of (23) for l can be expressed as

$$\begin{cases} Q(l') - V_j(l') \le l < Q(l') - \tilde{V}_{j-1}(l'), \text{ or} \\ Q(l') + \tilde{V}_{j-1}(l') < l \le Q(l') + V_j(l) \end{cases} \tag{27}$$

where

$$\tilde{V}_{j-1}(l') = \begin{cases} \sqrt{u_{j-1}^2 - B(l')}, & \text{if } B(l') \le u_{j-1}^2 \\ 0, & \text{if } B(l') > u_{j-1}^2 \end{cases} \tag{28}$$

$$V_j(l') = \begin{cases} \sqrt{u_j^2 - B(l')}, & \text{if } B(l') \le u_j^2 \\ \text{non-causal}, & \text{if } B(l') > u_j^2 \end{cases} \tag{29}$$

By virtue of (24), the integral (20) becomes

$$\begin{aligned} I(l_m^p, l_n^q) = & \int_0^{l_m^p} \int_{\max[0, P(l) - U_j(l)]}^{\min\left[l_n^q, P(l) - \tilde{U}_{j-1}(l)\right]} h(l, l') dl' dl \\ & + \int_0^{l_m^p} \int_{\max\left[0, P(l) + \tilde{U}_{j-1}(l)\right]}^{\min\left[l_n^q, P(l) + U_j(l)\right]} h(l, l') dl' dl \end{aligned} \tag{30}$$

Now, we concentrate on dealing with the first term in (30), as the second term can be treated in the same way. The integral with respect to l' is

$$\psi(l) \triangleq \int_{\max\left[0,P(l)-U_j(l)\right]}^{\min\left[l_n^q,P(l)-\tilde{U}_{j-1}(l)\right]} h(l,l')dl' =$$

$$\begin{cases} \int_0^{l_n^q} h(l,l')dl', & \text{if } l_n^q + \tilde{U}_{j-1}(l) < P(l) \le U_j(l) \\ \int_0^{P(l)-\tilde{U}_{j-1}(l)} h(l,l')dl', & \text{if } \tilde{U}_{j-1}(l) < P(l) < \min\left[U_j(l),\ l_n^q + \tilde{U}_{j-1}(l)\right] \\ \int_{P(l)-U_j(l)}^{l_n^q} h(l,l')dl', & \text{if } \max\left[U_j(l),\ l_n^q + \tilde{U}_{j-1}(l)\right] < P(l) < l_n^q + U_j(l) \\ \int_{P(l)-U_j(l)}^{P(l)-\tilde{U}_{j-1}(l)} h(l,l')dl', & \text{if } U_j(l) \le P(l) < l_n^q + \tilde{U}_{j-1}(l) \end{cases} \tag{31}$$

The inequalities in (31) have to be solved to determine the integrating bounds with respect to l. To illustrate the process to solve $l_n^q + \tilde{U}_{j-1}(l) < P(l) \le U_j(l)$, please refer to Figure 3, in which x and y are used to stand for l and l', respectively. From Figure 3(a), we have

$$\begin{aligned} &\tilde{b} + \tilde{U}_{j-1}(x) < P(x) \\ \Rightarrow \tilde{\Omega} \triangleq &\begin{cases} \tilde{x}_c < x < \infty, & \text{for case 0} \\ \tilde{x}_c < x < \tilde{x}_1 \text{ or } \tilde{x}_2 < x < \infty, & \text{for case 1: } \tilde{x}_c < \tilde{x}_{01} \\ \tilde{x}_2 < x < \infty, & \text{for case 2: } \tilde{x}_{01} \le \tilde{x}_c < \tilde{x}_{02} \\ \tilde{x}_c < x < \infty, & \text{for case 3: } \tilde{x}_c \ge \tilde{x}_{02} \end{cases} \end{aligned} \tag{32}$$

where $\tilde{x}_c = (\tilde{b} + \xi)/\alpha$ with $\tilde{b} = 0$ or l_n^q; $\tilde{x}_1$ and $\tilde{x}_2$ are the solutions of $\tilde{b} + \tilde{U}_{j-1}(x) = P(x)$ that gives $\tilde{x}_{1,2} = Q(\tilde{b}) \mp \tilde{V}_{j-1}(\tilde{b})$ with $Q(*)$ and $\tilde{V}_{j-1}(*)$ defined in (22) and (28); $\tilde{x}_{01}$ and $\tilde{x}_{02}$ are the roots of $\tilde{U}_{j-1}(x) = 0$, i.e., $\tilde{x}_{01,02} = x_0 \mp \sqrt{u_{j-1}^2 - A_0/(1-\alpha^2)}$ with $x_0 = -(\alpha\xi+\eta)/(1-\alpha^2)$ and $A_0 = (d^2 - \xi^2) - (1-\alpha^2)x_0^2$. Case 0 is actually a special case of case 1 when $\tilde{V}_{j-1}(\tilde{b}) = 0$ so that $\tilde{x}_1 = \tilde{x}_2$ results. Similarly, from Figure 3(b), we have

$$P(x) \le b + U_j(x) \Rightarrow \Omega \triangleq \begin{cases} \text{non-causal}, & \text{for case 0} \\ x_1 \le x \le x_2, & \text{for case 1: } x_c < x_{01} \\ x_{01} \le x \le x_2, & \text{for case 2: } x_{01} \le x_c < x_{02} \\ x_{01} \le x \le x_{02}, & \text{for case 3: } x_c \ge x_{02} \end{cases} \tag{33}$$

where $x_c = (b + \xi)/\alpha$ with $b = 0$ or l_n^q; x_1 and x_2 are the solutions of $b + U_j(x) = P(x)$ that gives $x_{1,2} = Q(b) \mp V_j(b)$; x_{01} and x_{02} are the

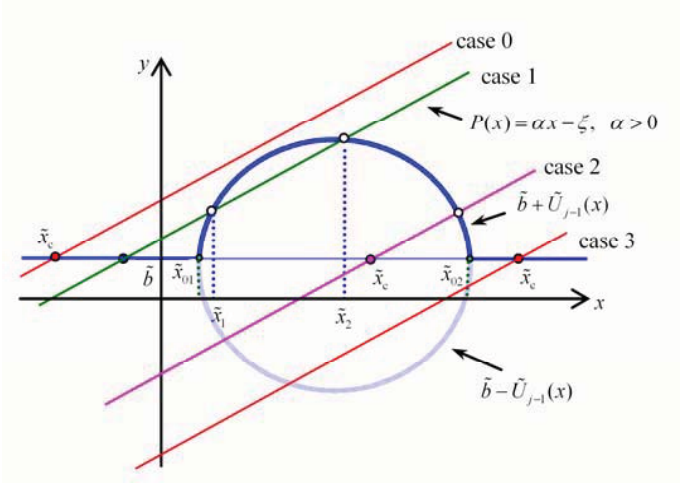

(a)

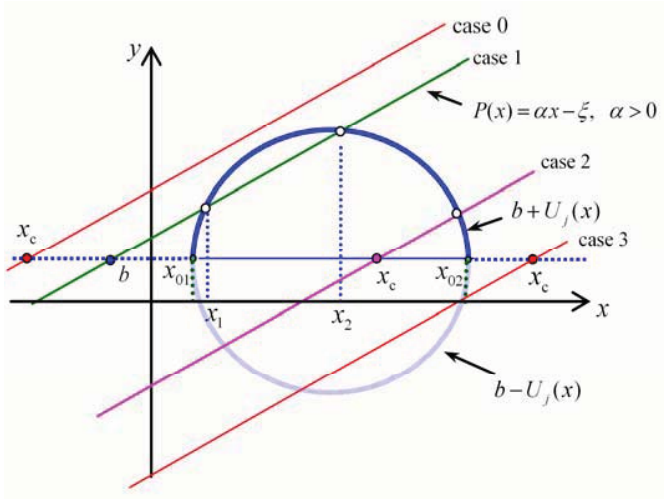

(b)

Figure 3. Illustration of solutions for (a) $\tilde{b}+\tilde{U}_{j-1}(x) < P(x)$, and (b) $P(x) \le b + U_j(x)$.

roots of $U_j(x) = 0$, i.e., $x_{01,02} = x_0 \mp \sqrt{u_j^2 - A_0/(1-\alpha^2)}$. Again, case 0 is actually a special case of case 1 when $V_j(b)$ violates causality so that the interval $x_1 \le x \le x_2$ vanishes.

By combining (32) and (33), the solution of inequality $l_n^q + \tilde{U}_{j-1}(l) < P(l) \le U_j(l)$ can be easily retrieved (by setting $\tilde{b} = l_n^q$

Table 1. The solution of $l_n^q + \tilde{U}_{j-1}(l) < P(l) \leq U_j(l)$, denoted by $D_1' = \tilde{\Omega} \cap \Omega$.

	$\tilde{x}_c < \tilde{x}_{01}$	$\tilde{x}_{01} \leq \tilde{x}_c < \tilde{x}_{02}$	$\tilde{x}_c \geq \tilde{x}_{02}$
$x_c < x_{01}$	$\max[\tilde{x}_c, x_1] < l < \min[\tilde{x}_1, x_2]$ or $\max[\tilde{x}_2, x_1] < l \leq x_2$	$\max[\tilde{x}_2, x_1] < l \leq x_2$	$\max[\tilde{x}_c, x_1] < l \leq x_2$
$x_{01} \leq x_c < x_{02}$	$\max[\tilde{x}_c, x_{01}] < l < \min[\tilde{x}_1, x_{02}]$ or $\max[\tilde{x}_2, x_{01}] < l \leq x_2$	$\max[\tilde{x}_2, x_{01}] < l \leq x_2$	$\max[\tilde{x}_c, x_{01}] < l \leq x_2$
$x_c \geq x_{02}$	$\max[\tilde{x}_c, x_{01}] < l < \min[\tilde{x}_1, x_{02}]$ or $\max[\tilde{x}_2, x_{01}] < l \leq x_{02}$	$\max[\tilde{x}_2, x_{01}] < l \leq x_{02}$	$\max[\tilde{x}_c, x_{01}] < l \leq x_{02}$

and $b = 0$) and denoted by $D_1' = \tilde{\Omega} \cap \Omega$, as listed in Table 1. Thus, along with $0 \leq l \leq l_m^p$, the integrating intervals for variable l is $D_1 = [0, l_m^p] \cap D_1'$. For the other three cases in (31), the integrating intervals for the variable l, denoted by D_2, D_3, D_4, respectively, can be determined by similar ways and not repeated for conciseness.

As a result, the first term of (30), with x and y standing for l and l', respectively, becomes

$$\int_{D_1} dx \int_0^{l_n^q} h(x,y)dy + \int_{D_2} dx \int_0^{P(x)-\tilde{U}_{j-1}(x)} h(x,y)dy + \int_{D_3} dx \int_{P(x)-U_j(x)}^{l_n^q} h(x,y)dx + \int_{D_4} dx \int_{P(x)-U_j(x)}^{P(x)-\tilde{U}_{j-1}(x)} h(x,y)dy \quad (34)$$

These integrals can be evaluated in closed-form ways. To check the correctness, we take the first term as an example and assume $\hat{s}_m^p = \hat{s}_n^q$, so that $\alpha = 1$, $\xi = -\eta$, $P(l) = l - \xi$, $Q(l') = l' + \xi$ and $A(l) = B(l') = d^2 - \xi^2$. It follows

$$\begin{aligned} & l_n^q + \tilde{U}_{j-1}(l) < P(l) \leq U_j(l) \\ \Rightarrow \quad & l_n^q + \sqrt{u_{j-1}^2 - (d^2 - \xi^2)} < l - \xi \leq \sqrt{u_j^2 - (d^2 - \xi^2)} \\ \Rightarrow \quad & (l_n^q + \xi) + \sqrt{u_{j-1}^2 - (d^2 - \xi^2)} < l \leq \xi + \sqrt{u_j^2 - (d^2 - \xi^2)} \end{aligned} \quad (35)$$

If we use (32) and (33) (by setting $\tilde{b} = l_n^q$ and $b = 0$), we have $\tilde{x}_c = l_n^q + \xi$, $\tilde{x}_{01,02} = \mp\infty$, $\tilde{x}_{1,2} = (l_n^q + \xi) \mp \sqrt{u_{j-1}^2 - (d^2 - \xi^2)}$; $x_c = \xi$, $x_{01,02} = \mp\infty$, $x_{1,2} = \xi \mp \sqrt{u_j^2 - (d^2 - \xi^2)}$. Thus, we find $\tilde{x}_{01} < \tilde{x}_c < \tilde{x}_{02}$

and $x_{01} < x_c < x_{02}$, and then by looking up Table 1 to obtain

$$\begin{aligned} & \max[\tilde{x}_2, x_{01}] < l \le x_2 \\ \Rightarrow \quad & (l_n^q + \xi) + \sqrt{u_{j-1}^2 - (d^2 - \xi^2)} < l \le \xi + \sqrt{u_j^2 - (d^2 - \xi^2)} \end{aligned}$$

which is identical to (35). Furthermore, if we let $h(x, y) = (xy)/R$ with $R = \sqrt{[y - (x - \xi)]^2 + (d^2 - \xi^2)}$, the first term of (34) reads

$$\int_{\max[0,\tilde{x}_2]}^{\min[l_m^p, x_2]} x dx \int_0^{l_n^q} \frac{y dy}{\sqrt{[y - (x - \xi)]^2 + (d^2 - \xi^2)}} = \int_{\max[0,\tilde{x}_2]}^{\min[l_m^p, x_2]} x dx$$
$$\left[\begin{array}{l} \sqrt{[y - (x - \xi)]^2 + (d^2 - \xi^2)} \\ -(x - \xi) \ln \left(\sqrt{[y - (x - \xi)]^2 + (d^2 - \xi^2)} - [y - (x - \xi)] \right) \end{array} \right]_{y=0}^{y=l_n^q}$$

which can be integrated analytically by using the following formulae (letting $z = y - (x - \xi)$ and $C = d^2 - \xi^2$):

$$\int z^\sigma \sqrt{z^2 + C}\, dz =$$
$$\begin{cases} \frac{z}{2}\sqrt{z^2 + C} + \frac{C}{2} \ln \left[\sqrt{z^2 + C} + z \right], & \sigma = 0 \\ \frac{1}{3} \left[z^2 + C \right]^{3/2}, & \sigma = 1 \\ \frac{z}{8}(2z^2 + C)\sqrt{z^2 + C} - \frac{C^2}{8} \ln \left[\sqrt{z^2 + C} + z \right], & \sigma = 2 \end{cases} \tag{36}$$

$$\int z^\sigma \ln \left[\sqrt{z^2 + C} - z \right] dx =$$
$$\begin{cases} \sqrt{z^2 + C} + z \ln \left[\sqrt{z^2 + C} - z \right], & \sigma = 0 \\ \frac{z}{4}\sqrt{z^2 + C} + \frac{z^2}{2} \ln \left[\sqrt{z^2 + C} - z \right] - \frac{C}{4} \ln \left[\sqrt{z^2 + C} + z \right], & \sigma = 1 \\ \frac{1}{9}(z^2 - 2C)\sqrt{z^2 + C} + \frac{z^3}{3} \ln \left[\sqrt{z^2 + C} - z \right], & \sigma = 2 \end{cases} \tag{37}$$

Following the procedure described above, the other three terms in (34) can also be evaluated analytically, which completes the first term in (30). The second term in (30) can be treated in the same way. Finally, full of the matrix elements are obtained via exact closed-form formulae.

4. NUMERICAL RESULTS

The first example is a dipole antenna illuminated by a Gaussian impulse [25]

$$\mathbf{E}^i(\mathbf{r},t) = \mathbf{E}_0 \frac{4}{T\sqrt{\pi}} \exp\left[-\frac{4}{T}\left(ct - ct_0 - \hat{k}\cdot\mathbf{r}\right)^2\right] \tag{38}$$

with $\mathbf{E}_0 = \hat{z}$, $T = 4$ and $ct_0 = 6$. The antenna is along the z-axis, has a length 1 m and radius 0.5 cm, and is divided into 10 segments. $\Delta t = \Delta z/c$ is used in this example. The short-circuit

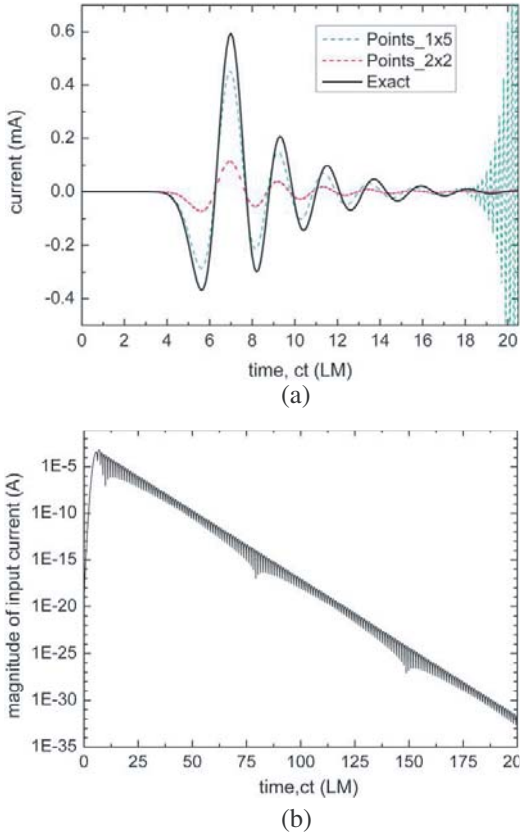

Figure 4. Currents at the center of the dipole: (a) comparison of inaccurate results obtained via numerical integration with exact results obtained via analytical formulae, and (b) decaying behavior of the current magnitude.

current at the center of the dipole is depicted in Figure 4(a) from 0 to 20 LM (LM = light meter: the time that light takes to travel 1 m in vacuum). For comparison, Figure 4(a) also contains two sets of conventional MOT results obtained by using Gaussian quadrature, in which Points_$M \times N$ means using M-point rule for the integration with respect to l and N-point rule for l'. It can be seen that the results are divergent or inaccurate if the number of integration points are not enough. It may be shown that the results will approach the exact results as the number of integration points is continuously increased. However, it is not known a priori that how many integration points are sufficient for convergence or for an acceptable accuracy. To inspect the late-time behavior, the magnitude of current is plotted in logarithm scale as shown in Figure 4(b) from 0 to 200 LM (4,000 time-steps). It can be seen that the current decays exponentially, which implies an

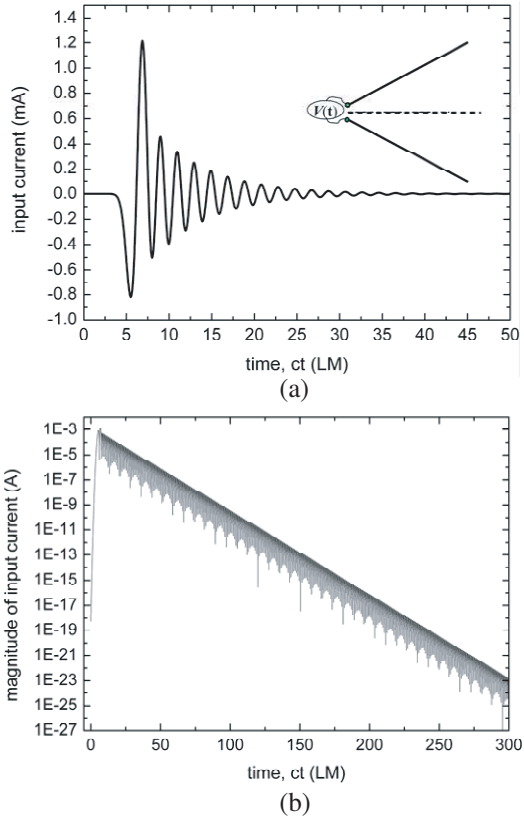

Figure 5. Radiation of a V-shape antenna: (a) input current, (b) decaying behavior of the input current.

absolute convergence for this example.

The second example is to analyze a radiation problem by a V-shaped antenna [25], which lies in the xy-plane and symmetrically about the x-axis, with the vertex at the origin. Each arm has a length of 0.5 m and is divided into ten segments. The radius of the arms is 0.5 cm. The included angle between the arms is 60°. A Gaussian source voltage

$$V(t) = \frac{4}{T\sqrt{\pi}} \exp\left[-\frac{4}{T}(ct - ct_0)^2\right] \tag{39}$$

is applied at the vertex (feed point), which enters (10) to yield $V_m^i = V(i\Delta t)$ if $m = (N+1)/2$ and $V_m^i = 0$ otherwise. The input current at the feed point for the time from 0 to 50 LM is displayed in Figure 5(a), and its late-time behavior till 300 LM (6,000 time-steps) is shown in Figure 5(b). It can be seen that the input current is also exponentially convergent but at a lower rate than the straight dipole antenna example above.

The third example is a radiation problem by a monopole helical beam antenna as shown in Figure 6. It has 6 turns and the pitch angle is 14 degrees. The 6-turn helix has a length of 1.24 m, and each turn is divided into ten segments. By using the image theory, the ground plane can be removed and a dipole helical antenna is considered instead. A Gaussian source voltage in (39) is applied at the feed point. The input current is depicted in Figure 6(a) till 8,300 LM (200,000 time-steps), which again decays exponentially but at much lower rate than the above dipole antenna and V-shaped antenna problems. Figure 6(b) shows the radiating far-field component E_x in the axis direction, which has a very long tail compared with the excitation waveform.

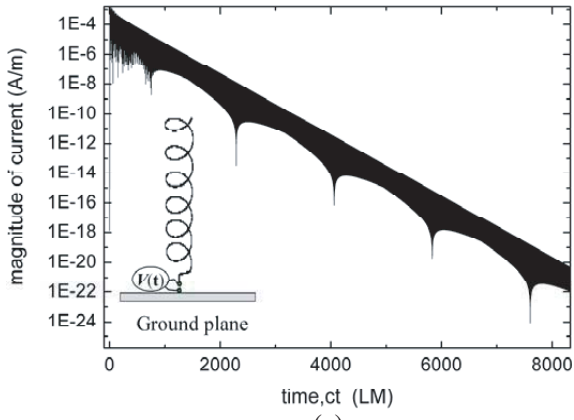

(a)

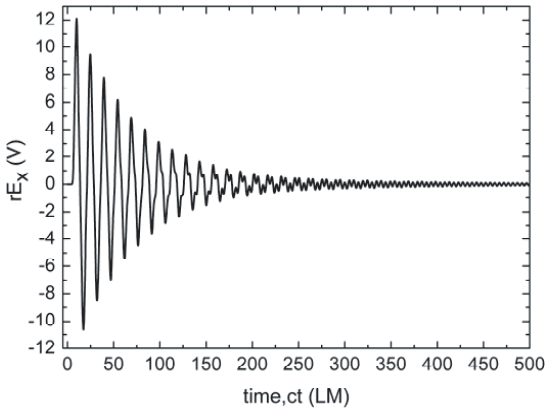

(b)

Figure 6. Radiation of a helical beam antenna: (a) decaying behavior of the input current, (b) the radiating far-field.

5. CONCLUDING REMARKS

A novel time-domain integral equation (TDIE) solver via exact calculations of full matrix elements for transient analysis of conducting wires is developed. Numerical examples show that the responses of currents to an impulse incident wave or an impulse excitation voltage attenuate exponentially, at some rate pertinent to the structures. The marching-on-in-time (MOT) process based on the present formulations with exact matrix elements seems to be immune to instability without sacrifice of accuracy or efficiency.

ACKNOWLEDGMENT

This work is supported by NSFC Project 60771001 and 60825102.

REFERENCES

1. Rynne, B. P., "Time domain scattering from arbitrary surfaces using the electric field integral equation," *Journal of Electromagnetic Waves and Applications*, Vol. 5, 93–112, 1991.
2. Rao, S. M., *Time Domain Electromagnetics*, Academic Press, 1999.
3. Sachdeva, N., S. M. Rao, and N. Balakrishnan, "A comparison of FDTD-PML with TDIE," *IEEE T. Antenn. Propag.*, Vol. 50, 1609–1614, 2002.

4. Zhang, G. H., M. Y. Xia, and C. H. Chan, "Time domain integral equation approach for analysis of transient responses by metallic-dielectric composite bodies," *Progress In Electromagnetics Research*, PIER 87, 1–14, 2008.
5. Ergin, A. A., B. Shanker, and E. Michielssen, "The plane wave time-domain algorithm for the fast analysis of transient wave phenomena," *IEEE T. Antenn. Propag.*, Vol. 41, 39–52, 1999.
6. Zhou, Z. X. and J. S. Tyo, "An adaptive time-domain integral equation method for transient analysis of wire scatterer," *IEEE T. Antenn. Propag.*, Vol. 4, 147–150, 2005.
7. Courant, R., K. Friedrichs, and H. Lewy, "On the partial difference equations of mathematical physics," *IBM J.*, Vol. 11, 215–234, 1967.
8. Sadigh, A. and E. Arvas, "Treating the instabilities in marching-on-in-time method from a different perspective," *IEEE T. Antenn. Propag.*, Vol. 41, 1695–1702, 1993.
9. Davies, P. J. and D. B. Duncan, "Averaging techniques for time-marching schemes for retarded potential integral equations," *App. Numer. Math.*, Vol. 23, 291–310, 1997.
10. Rynne, B. P. and P. D. Smith, "Stability of time-marching algorithms for electric field integral equation," *Journal of Electromagnetic Waves and Applications*, Vol. 4, 1181–1205, 1990.
11. Rao, S. M. and T. K. Sarkar, "Transient analysis of electromagnetic scattering from wire structures utilizing an implicit time-domain integral equation technique," *Microw. Opt. Technol. Lett.*, Vol. 17, 66–69, 1998.
12. Shifman, Y. and Y. Leviatan, "On the use of spatiotemporal multiresolution analysis in method of moments solutions for the time-domain integral equation," *IEEE T. Antenn. Propag.*, Vol. 49, 1123–1129, 2001.
13. Jung, B. H., J. Zhong, T. K. Sarkar, and M. Salazar-Palma, "A comparison of marching-on in time method with marching-on in degree method for the TDIE solver," *Progress In Electromagnetics Research*, PIER 70, 281–296, 2007.
14. Jung, B. H., Y.-S. Chung, and T. K. Sarkar, "Time-domain EFIE, MFIE, and CFIE formulations using Laguerre polynomials as temporal basis functions for the analysis of transient scattering from arbitrary shaped conducting structures," *Progress In Electromagnetics Research*, PIER 39, 1–45, 2003.
15. Andriulli, F. P. and E. Michielssen, "A regularized combined field integral equation for scattering from 2-D perfect electrically

conducting objects," *IEEE T. Antenn. Propag.*, Vol. 55, 2522–2529, 2007.

16. Manara, G., A. Monorchio, and R. Reggiannini, "A space-time discretization criterion for a stable time-marching solution of the electric field integral equation," *IEEE T. Antenn. Propag.*, Vol. 45, 527–532, 1997.
17. Hu, J. L., C. H. Chan, and Y. Xu, "A new temporal basis function for the time domain integral equation method," *IEEE Microw. Wireless Comp. Lett.*, Vol. 11, 465–466, 2001.
18. Xia, M. Y., G. H. Zhang, G. L. Dai, et al., "Stable solution of time domain integral equation methods using quadratic B-spline temporal basis functions," *J. Comput. Math.*, Vol. 25, 374–384, 2007.
19. Bagci, H., A. E. Yilmaz, V. Lomakin, and E. Michielssen, "Fast solution of mixed-potential time-domain integral equations for half-space environments," *IEEE T. Geosci. Remote Sensing*, Vol. 43, 269–279, 2005.
20. Lu, M. and E. Michielssen, "Closed form evaluation of time domain fields due to Rao-Wilton-Glisson sources for use in marching-on-in-time based EFIE solvers," *IEEE APS. Int. Symp. Dig.*, 74–77, 2002.
21. Pingenot, J., S. Chakraborty, and V. Jandhyala, "Polar integration for exact space-time quadrature in time-domain integral equations," *IEEE Trans. Antenn. Propag.*, Vol. 54, 3037–3042, 2006.
22. Zubik-Kowal, B. and P. J. Davies, "Numerical approximation of time domain electromagnetic scattering from a thin wire," *Numerical Algorithms*, Vol. 30, 25–35, 2002.
23. Bayer, S. E. and A. A.Ergin, "A stable marching-on-in-time scheme for wire scatterers using a newmark-beta formulation," *Progress In Electromagnetics Research B*, Vol. 6, 337–360, 2008.
24. Rao, S. M., D. R. Wilton, and A. W. Glisson, "Electromagnetic scattering by surfaces of arbitrary shape," *IEEE T. Antenn. Propag.*, Vol. 30, 409–418, 1982.
25. Zhong, J., T. K. Sarkar, B. H. Jung, Y.-S. Chung, et al., "A stable solution of time domain electric field integral equation for thin-wire antennas using the Laguerre polynomials," *IEEE T. Antenn. Propag.*, Vol. 52, 2641–2649, 2004.